INSTITUTE OF PHYSICS PUBLISHING CLASSICAL AND QUANTUM GRAVITY

Class. Quantum Grav. **23** (2006) S29–S39 doi:10.1088/0264-9381/23/8/S05

Search for gravitational-wave bursts in LIGO's third science run

B Abbott[1], R Abbott[1], R Adhikari[1], J Agresti[1], P Ajith[2], B Allen[3], J Allen[4], R Amin[5], S B Anderson[1], W G Anderson[3], M Araya[1], H Armandula[1], M Ashley[6], C Aulbert[7], S Babak[7], R Balasubramanian[8], S Ballmer[4], H Bantilan[9], B C Barish[1], C Barker[10], D Barker[10], M A Barton[1], K Bayer[4], K Belczynski[11,42], J Betzwieser[4], B Bhawal[1], I A Bilenko[12], G Billingsley[1], E Black[1], K Blackburn[1], L Blackburn[4], B Bland[10], L Bogue[13], R Bork[1], S Bose[14], P R Brady[3], V B Braginsky[12], J E Brau[15], D A Brown[1], A Buonanno[16], D Busby[1], W E Butler[17], L Cadonati[4], G Cagnoli[18], J B Camp[19], J Cannizzo[19], K Cannon[3], J Cao[4], L Cardenas[1], K Carter[13], M M Casey[18], P Charlton[1,43], S Chatterji[1], Y Chen[7], D Chin[20], N Christensen[9], T Cokelaer[8], C N Colacino[21], R Coldwell[22], D Cook[10], T Corbitt[4], D Coyne[1], J D E Creighton[3], T D Creighton[1], J Dalrymple[23], E D'Ambrosio[1], K Danzmann[2,24], G Davies[8], D DeBra[25], V Dergachev[20], S Desai[6], R DeSalvo[1], S Dhurandar[35], M Díaz[26], A Di Credico[23], R W P Drever[27], R J Dupuis[1], P Ehrens[1], T Etzel[1], M Evans[1], T Evans[13], S Fairhurst[3], L S Finn[6], K Y Franzen[22], R E Frey[15], P Fritschel[4], V V Frolov[13], M Fyffe[13], K S Ganezer[28], J Garofoli[10], I Gholami[7], J A Giaime[5], K Goda[4], L Goggin[1], G González[5], C Gray[10], A M Gretarsson[29], D Grimmett[1], H Grote[2], S Grunewald[7], M Guenther[10], R Gustafson[20], W O Hamilton[5], C Hanna[5], J Hanson[13], C Hardham[25], G Harry[4], J Heefner[1], I S Heng[18], M Hewitson[2], N Hindman[10], P Hoang[1], J Hough[18], W Hua[25], M Ito[15], Y Itoh[3], A Ivanov[1], B Johnson[10], W W Johnson[5], D I Jones[6,44], G Jones[8], L Jones[1], V Kalogera[11], E Katsavounidis[4], K Kawabe[10], S Kawamura[30], W Kells[1], A Khan[13], C Kim[11], P King[1], S Klimenko[22], S Koranda[3], D Kozak[1], B Krishnan[7], M Landry[10], B Lantz[25], A Lazzarini[1], M Lei[1], I Leonor[15], K Libbrecht[1], P Lindquist[1], S Liu[1], M Lormand[13], M Lubinski[10], H Lück[2], M Luna[31], B Machenschalk[7], M MacInnis[4], M Mageswaran[1], K Mailand[1], M Malec[24], V Mandic[1], S Márka[32], E Maros[1], K Mason[4], L Matone[32], N Mavalvala[4], R McCarthy[10], D E McClelland[33], M McHugh[34], J W C McNabb[6], A Melissinos[17], G Mendell[10], R A Mercer[21], S Meshkov[1], E Messaritaki[3], C Messenger[21], E Mikhailov[4], S Mitra[35], V P Mitrofanov[12], G Mitselmakher[22], R Mittleman[4], O Miyakawa[1], S Mohanty[26], G Moreno[10], K Mossavi[2], G Mueller[22], S Mukherjee[26], E Myers[36], J Myers[10], T Nash[1], F Nocera[1], J S Noel[14], B O'Reilly[13], R O'Shaughnessy[11], D J Ottaway[4], H Overmier[13], B J Owen[6], Y Pan[37], M A Papa[7], V Parameshwaraiah[10],

[42] Present address: New Mexico State University, USA.
[43] Present address: Charles Sturt University, Australia.
[44] Present address: University of Southampton, UK.

0264-9381/06/080029+11$30.00

C Parameswariah[13,45], M Pedraza[1], S Penn[38], M Pitkin[18], R Prix[7], V Quetschke[22], F Raab[10], H Radkins[10], R Rahkola[15], M Rakhmanov[22], K Rawlins[4,46], S Ray-Majumder[3], V Re[21], T Regimbau[8,47], D H Reitze[22], R Riesen[13], K Riles[20], B Rivera[10], D I Robertson[18], N A Robertson[18,25], C Robinson[8], S Roddy[13], A Rodriguez[5], J Rollins[32], J D Romano[8], J Romie[1], S Rowan[18], A Rüdiger[2], L Ruet[4], P Russell[1], K Ryan[10], V Sandberg[10], G H Sanders[1,48], V Sannibale[1], P Sarin[4], B S Sathyaprakash[8], P R Saulson[23], R Savage[10], A Sazonov[22], R Schilling[2], R Schofield[15], B F Schutz[7], P Schwinberg[10], S M Scott[33], S E Seader[14], A C Searle[33], B Sears[1], D Sellers[13], A S Sengupta[8], P Shawhan[1], D H Shoemaker[4], A Sibley[13], X Siemens[3], D Sigg[10], A M Sintes[7,31], J Smith[2], M R Smith[1], O Spjeld[13], K A Strain[18], D M Strom[15], A Stuver[6], T Summerscales[6], M Sung[5], P J Sutton[1], D B Tanner[22], M Tarallo[1], R Taylor[1], K A Thorne[6], K S Thorne[37], K V Tokmakov[12], C Torres[26], C Torrie[1], G Traylor[13], W Tyler[1], D Ugolini[39], C Ungarelli[21], M Vallisneri[37], M van Putten[4], S Vass[1], A Vecchio[21], J Veitch[18], C Vorvick[10], S P Vyachanin[12], L Wallace[1], H Ward[18], R Ward[1], K Watts[13], D Webber[1], U Weiland[24], A Weinstein[1], R Weiss[4], S Wen[5], K Wette[33], J T Whelan[34], S E Whitcomb[1], B F Whiting[22], S Wiley[28], C Wilkinson[10], P A Willems[1], B Willke[2,24], A Wilson[1], W Winkler[2], S Wise[22], A G Wiseman[3], G Woan[18], D Woods[3], R Wooley[13], J Worden[10], I Yakushin[13], H Yamamoto[1], S Yoshida[40], M Zanolin[4], L Zhang[1], N Zotov[41], M Zucker[13] and J Zweizig[1] (LIGO Scientific Collaboration)

[1] LIGO—California Institute of Technology, Pasadena, CA 91125, USA
[2] Albert-Einstein-Institut, Max-Planck-Institut für Gravitationsphysik, D-30167 Hannover, Germany
[3] University of Wisconsin-Milwaukee, Milwaukee, WI 53201, USA
[4] LIGO—Massachusetts Institute of Technology, Cambridge, MA 02139, USA
[5] Louisiana State University, Baton Rouge, LA 70803, USA
[6] The Pennsylvania State University, University Park, PA 16802, USA
[7] Albert-Einstein-Institut, Max-Planck-Institut für Gravitationsphysik, D-14476 Golm, Germany
[8] Cardiff University, Cardiff CF2 3YB, UK
[9] Carleton College, Northfield, MN 55057, USA
[10] LIGO Hanford Observatory, Richland, WA 99352, USA
[11] Northwestern University, Evanston, IL 60208, USA
[12] Moscow State University, Moscow 119992, Russia
[13] LIGO Livingston Observatory, Livingston, LA 70754, USA
[14] Washington State University, Pullman, WA 99164, USA
[15] University of Oregon, Eugene, OR 97403, USA
[16] University of Maryland, College Park, MD 20742 USA
[17] University of Rochester, Rochester, NY 14627, USA
[18] University of Glasgow, Glasgow G12 8QQ, UK
[19] NASA/Goddard Space Flight Center, Greenbelt, MD 20771, USA
[20] University of Michigan, Ann Arbor, MI 48109, USA
[21] University of Birmingham, Birmingham B15 2TT, UK
[22] University of Florida, Gainesville, FL 32611, USA
[23] Syracuse University, Syracuse, NY 13244, USA

[45] Present address: New Mexico Institute of Mining and Technology/Magdalena Ridge Observatory Interferometer, USA.
[46] Present address: University of Alaska Anchorage, USA.
[47] Present address: Observatoire de la Côte d'Azur, France.
[48] Present address: Thirty Meter Telescope Project, Caltech, USA.

[24] Universität Hannover, D-30167 Hannover, Germany
[25] Stanford University, Stanford, CA 94305, USA
[26] The University of Texas at Brownsville and Texas Southmost College, Brownsville, TX 78520, USA
[27] California Institute of Technology, Pasadena, CA 91125, USA
[28] California State University Dominguez Hills, Carson, CA 90747, USA
[29] Embry-Riddle Aeronautical University, Prescott, AZ 86301, USA
[30] National Astronomical Observatory of Japan, Tokyo 181-8588, Japan
[31] Universitat de les Illes Balears, E-07122 Palma de Mallorca, Spain
[32] Columbia University, New York, NY 10027, USA
[33] Australian National University, Canberra 0200, Australia
[34] Loyola University, New Orleans, LA 70118, USA
[35] Inter-University Centre for Astronomy and Astrophysics, Pune 411007, India
[36] Vassar College, Poughkeepsie, NY 12604, USA
[37] Caltech-CaRT, Pasadena, CA 91125, USA
[38] Hobart and William Smith Colleges, Geneva, NY 14456, USA
[39] Trinity University, San Antonio, TX 78212, USA
[40] Southeastern Louisiana University, Hammond, LA 70402, USA
[41] Louisiana Tech University, Ruston, LA 71272, USA

Received 14 October 2005, in final form 29 November 2005
Published 22 March 2006
Online at stacks.iop.org/CQG/23/S29

Abstract
We report on a search for gravitational-wave bursts in data from the three LIGO interferometric detectors during their third science run. The search targets sub-second bursts in the frequency range 100–1100 Hz for which no waveform model is assumed and has a sensitivity in terms of the *root-sum-square* (rss) strain amplitude of $h_{\mathrm{rss}} \sim 10^{-20}$ $\mathrm{Hz}^{-1/2}$. No gravitational-wave signals were detected in the eight days of analysed data.

PACS numbers: 04.80.Nn, 07.05.Kf, 95.30.Sf, 95.85.Sz

1. Introduction

Gravitational-wave bursts are generally described as time-varying strain signals that are of very short duration. Within the context of LIGO data analysis, this term describes primarily sub-second duration signals with significant power in the instruments' sensitive frequency band. Typical sources of this kind of radiation include astrophysical systems for which the resulting burst waveforms are either poorly modelled or are completely unknown. These include the core collapse of massive stars, the merger phase of binary black-hole systems and the astrophysical engines that power gamma-ray bursts. Other sources of gravitational-wave bursts exist for which their waveforms are well modelled. These include black-hole ringdowns and bursts resulting from cosmic string cusps and kinks. Gravitational-wave bursts may also result from sources that are completely unknown or not anticipated.

The Laser Interferometer Gravitational wave Observatory (LIGO) is a network of interferometric detectors aiming to make direct observations of gravitational waves [1]. LIGO is composed of three interferometers at two sites. Two interferometers, one of 4 km (H1) and another of 2 km arm length (H2), are co-located at Hanford, WA. A third instrument of 4 km arm length (L1) is located at Livingston, LA. Each detector is a power-recycled Michelson

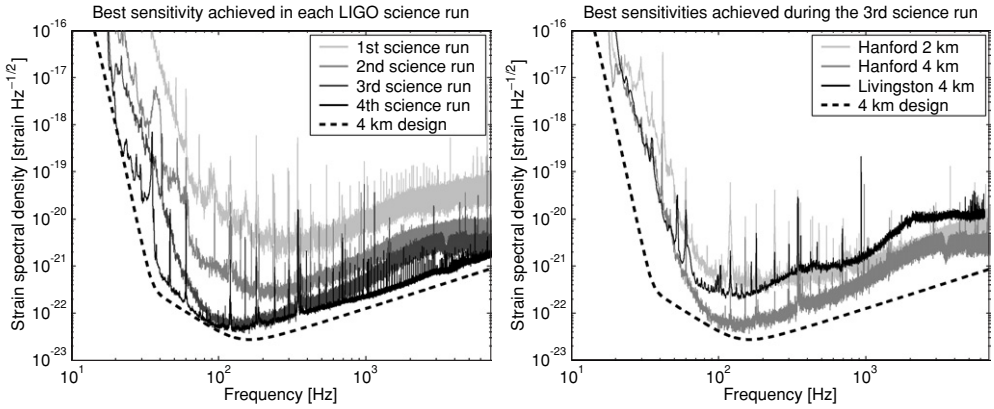

Figure 1. Left plot: sensitivity progress of the LIGO 4 km interferometers. The traces show the best sensitivity achieved by either of the LIGO interferometers during each of the four LIGO science runs, along with the 4 km design sensitivity in the LIGO Science Requirements Document. Right plot: best sensitivity achieved by each LIGO interferometer during the third science run.

interferometer with Fabry–Perot cavities in each of its orthogonal arms. These interferometers are sensitive to quadrupolar oscillations in the spacetime metric due to passing gravitational waves.

LIGO commissioning has been interspersed with the collection of data under stable operating conditions in order to perform astrophysical gravitational-wave searches. The first science run, called S1, took place in the summer of 2002 (23 August–9 September), while two additional runs, S2 and S3, collected data in 2003 (S2: 14 February–14 April; S3: 31 October 2003–9 January 2004). A fourth science run, S4, took place at the beginning of 2005 (22 February–23 March). As of May 2005, the instruments are to within a factor of 2 of their design expectation in their most sensitive frequency band.

Three searches for gravitational-wave bursts were performed using data collected by the LIGO instruments in S1 and S2 [2–4]. These include the first *untriggered* search using 35.5 h of S1 data [2] and the first *triggered* search for gravitational-wave bursts in coincidence with one of the brightest GRBs, 030329, which fortuitously occurred during LIGO's S2 run [3]. In the most recent publication [4], the analysis of 239.5 h of data taken while the three LIGO detectors were in simultaneous operation during S2 was reported. As in the previous burst searches with the LIGO detectors, no final candidate events were observed and the search results were interpreted as an upper limit of 0.26 events per day on the rate of gravitational-wave bursts at the instruments at the 90% confidence level. The all-sky averaged sensitivity of the S2 search for bursts with significant power in the LIGO sensitivity band (100–1000 Hz) lies in the range of $h_{\rm rss} \sim 10^{-20}$–$10^{-19}$ Hz$^{-1/2}$ root-sum-square (rss) strain amplitude [4]. In this analysis we use data from the S3 run of the LIGO detectors in order to search for gravitational-wave bursts. The S3 run provided data with improved sensitivity with respect to the previous data taking, as can be seen in figure 1.

2. Search pipeline overview

The burst search pipeline for the S3 analysis follows closely the procedure used for the S2 search [4]. As in S2, the search is restricted to burst signals that are detectable above the noise in all three LIGO detectors at once. Therefore, we begin with times when the three detectors

are operating in 'science mode' simultaneously. This 'triple-coincident' data set is further reduced by removing periods of data taking when instrumental artefacts or environmental conditions have been shown to degrade the search.

The Waveburst [5] algorithm is used to identify coincident clusters of excess power in the wavelet domain across the three gravitational-wave data streams. The triggers generated by Waveburst are checked for amplitude consistency and then passed to the r-statistic [6] waveform consistency test, which uses a normalized cross-correlation statistic to check for consistent waveform morphology between pairs of detectors.

We estimate the background event rate from accidental noise sources (i.e., anything *not* directly causing a simultaneous event in the three detectors) by running the pipeline over time-shifted data where the gravitational-wave data stream from the Livingston detector is artificially shifted in time with respect to the two Hanford detectors. It is assumed that the time-shifted noise has similar characteristics to the unshifted noise, and that the instrumental behaviour is approximately stationary over the range of time shifts (up to 2 min). To check this assumption, we verify that the distribution of event counts at the various nonzero time shifts is consistent with a Poisson process. Detection efficiencies for a variety of ad hoc and model-based waveforms are measured by running the pipeline over the real detector data, with software injections added to the time series. The efficiencies measured are checked against those of physical hardware injections carried out during the run.

We tune the parameters of the search algorithms with the goal of maximizing detection efficiency over the simulated events while maintaining a very low false event rate. Unlike the S2 analysis, time-shifted data over the entire run is used for tuning instead of a random subset of 'playground' data set aside purely for such studies. This procedure avoids removing a valuable fraction of the data from the analysis result and reduces the chance that the playground data is unrepresentative of the entire data set. Once the thresholds and parameters of the search are decided, we run the pipeline over a new set of time shifts to estimate the background rate, as well as the unshifted data to search for candidate gravitational-wave events.

3. Data selection

There are 265.1 h of data with all three detectors operating simultaneously in science mode, giving a triple-coincident duty cycle of 16% over the S3 run. From these, 14.0 h (5.3%) are removed due to data-acquisition problems: unwritten data, data-acquisition overflows, and timing and synchronization errors.

A number of additional instrumental issues were discovered during the analysis and accounted for in the final data selection. First, we ignore the 10 s just before loss of optical cavity resonance in any of the interferometers, as such loss is often preceded by a sudden growth in instrument instability. Also, periods of excessive levels of dust at any of the output optical tables of the interferometers are removed from the analysis. Large transients in the gravitational-wave channel were found to occur during large fluctuations in the light level stored in the arm cavities; such periods are identified and removed. We implement two event-by-event vetoes that are used to remove single events that can be identified with observed instrumental artefacts. The first is a veto applied to all three detectors on events caused by a calibration line drop-out. The second is a veto for events occurring simultaneously with a large excursion in the power-recycling servo loop control signal for H2. Details on the selection and safety of the event-by-event vetoes can be found in the S3 data quality and veto paper [7]. In total, these cuts reduce the data set by an additional 16.8%.

The presence of a remaining environmental event at the end of the S2 burst analysis [4] underscored the need to monitor environmental disturbances. In the case of the S2 event,

strong coherent signals were acoustically coupled into the co-located H1 and H2 detectors when a propeller airplane flew overhead. Although the acoustic coupling was reduced for S3, airplane signals in the gravitational-wave channel were still observed during our investigations. To automate a search for these acoustical disturbances, we identify periods in many of the microphone channels with large RMS noise in the 62–100 Hz range. Periods of high acoustic activity are removed from the analysis at both sites. A similar RMS-based monitor is used on seismic data from the Hanford site to identify periods of high seismic activity at frequencies with large coupling to the mirrors. These two environmental cuts further reduce the data set by 1.5%.

The above data quality cuts remove 62.5 h from the original 265.1 h of triple-coincident livetime. The Waveburst algorithm is able to analyse 95% of the remaining 202.6 h, with some loss due to data stream segmentation and boundary effects of the wavelet transform, resulting in an effective S3 livetime of 192.2 h for this burst analysis.

4. Event generation

4.1. Trigger generation

The Waveburst algorithm [5], also used for the S2 analysis [8], generates triggers on coincident excess power in the wavelet domain across the raw gravitational-wave data streams. The data first undergo a complete wavelet packet decomposition, giving for each detector a uniform time–frequency map of the signal indexed in time by i and in frequency by j. Significant tiles in each decomposition are defined by the largest 10% of wavelet coefficients at each effective frequency. They are assigned a *significance* according to their energy-determined rank within the set of tiles at fixed frequency j:

$$y_{ij} = -\ln(R_{ij}/N), \tag{1}$$

where the rank, R_{ij}, is equal to 1 for the most energetic and N for the least energetic of the selected N tiles. The significant tiles with closely matching tiles in time and frequency across the three data streams are determined to be 'in coincidence', and a clustering routine clusters nearby tiles from the set of coincident tiles for each detector separately.

These single-detector clusters are thus built from the triple-coincident energy in the wavelet domain. Each cluster of k tiles, $C(k)$, is characterized by its *cluster significance*, z, given by

$$z = Y - \ln\left(\sum_{m=0}^{k-1} \frac{Y^m}{m!}\right), \qquad \text{where} \quad Y = \sum_{i,j \in C(k)} y_{ij}, \tag{2}$$

which has an exponential distribution regardless of cluster size. The *trigger significance*, Z_g, is calculated as the geometric average of the cluster significances for a particular H1/H2/L1 coincident triplet of clusters. Z_g provides a measure of the confidence of each triple-coincident event trigger and is used for future thresholding.

The Waveburst implementation used for S3 has two major improvements over the S2 version. For S2, Waveburst operated on just two data streams, meaning that for triple-coincidence analysis, the final triggers from the three detector pairs were subject to yet another coincidence stage. For S3, Waveburst is able to analyse an arbitrary number of data streams at once, allowing a tighter triple-coincidence stage prior to clustering. Also during the S2 analysis, Waveburst searched the wavelet time–frequency map at a fixed resolution of $1/128$ s $\times$ 64 Hz. While this was well tuned for a region of the parameter space of interest, other regions suffered from poor matching of the wavelet basis to simulated bursts, particularly

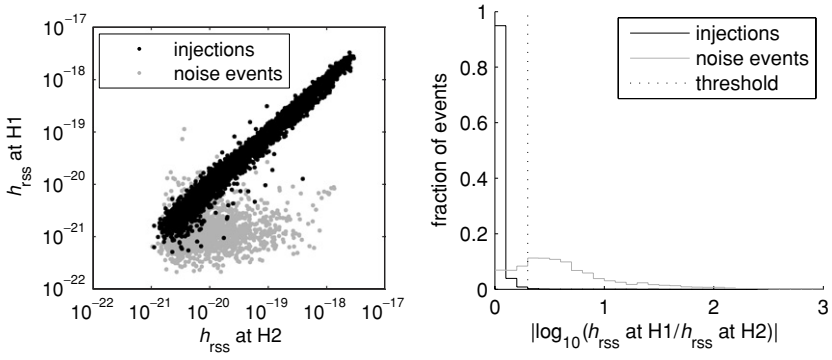

Figure 2. Waveburst h_{rss} amplitude consistency between H1 and H2 for injections of simulated signals and for time-shifted events. On the left is a scatter plot showing the recorded amplitudes at both detectors for each event. On the right is a histogram of the absolute value of the logarithm of the ratio of recorded amplitudes, with a dotted line showing the threshold chosen for an h_{rss} consistency within a factor of 2.

at low frequencies where the choice of simulated bursts included many waveforms longer than 1/128 s. For S3, Waveburst operates on several additional time–frequency resolutions, essentially running a separate analysis at each resolution and combining the results at the end. This allows for better matching of the time–frequency tiles to a much larger parameter space.

4.2. Amplitude consistency

Because the orientations of the two Hanford interferometers are identical, we expect to observe the same strain waveform at the two detectors. Simulations show that the accuracy of signal-energy reconstruction by Waveburst of a gravitational-wave burst is sufficient to use amplitude consistency to rule out spurious events. Based on the performance over simulated signals shown in figure 2, we require the observed h_{rss} amplitudes in the two Hanford detectors to agree within a factor of 2. This allows us to reject 76% of the time-shifted events while maintaining a false rejection rate of just 0.4% for simulated bursts.

4.3. Waveform consistency

We use the r-statistic test [6] to check for waveform consistency across the three detectors. The test is run over time intervals triggered by Waveburst as a means of further reducing the background rate. The test measures the normalized cross-correlation,

$$r = \frac{\sum_i (x_i - \bar{x})(y_i - \bar{y})}{\sqrt{\sum_i (x_i - \bar{x})^2}\sqrt{\sum_i (y_i - \bar{y})^2}}, \tag{3}$$

between two whitened gravitational-wave strain data time series $\{x_i\}$ and $\{y_i\}$ with mean values $\bar{x}$ and $\bar{y}$. For uncorrelated white noise of sufficient length N_p such that the central limit theorem applies, we expect the r-statistic values obtained to follow a normal distribution with zero mean and $\sigma_p = 1/\sqrt{N_p}$. Any coherent component in the two sequences will cause r to deviate from the normal distribution.

To compute the r-statistic for unknown waveform duration and sky position, we use integration lengths N_p corresponding to 20, 50 and 100 ms, which have been shown to cover well the burst durations of interest. The integration windows scan over a region surrounding the Waveburst trigger central time, calculating r using rectangular windows centred at each

time j. Furthermore, the two data streams may be shifted by a small amount, k, prior to calculating the r-statistic. For the H1–H2 pair, k is ± 1 ms to account for a small timing error, while for Hanford–Livingston pairs k takes on values up to ± 11 ms to account for all possible physical light travel times between the sites. For each pair of detectors, the maximum logarithmic confidence is obtained:

$$C = \max\left\{-\log_{10}\left[\operatorname{erfc}\left(|r_{pj}^{k}|\sqrt{\frac{N_p}{2}}\right)\right]\right\}. \tag{4}$$

The parameter Γ is then defined as the arithmetic average of the three values of C from the three detector pairs. This single parameter is used for thresholding to cut events with low confidence. A final requirement is that the sign of r at maximum confidence between H1 and H2 must be positive. Otherwise the trigger is discarded since a negative value would imply opposite phase. Because L1 is not precisely aligned with the Hanford detectors, it will be sensitive to different gravitational-wave polarizations and thus different waveforms. We therefore do not expect the signals to be 100% correlated between the sites. This is taken into account, in a waveform-dependent way, in our simulations.

5. Search results

Preliminary studies over time-shifted S3 data led us to set thresholds on the Waveburst $Z_{\mathrm{g}} \geqslant 7.39$ and r-statistic $\Gamma \geqslant 10$. To estimate the background rate at these thresholds, we run through the pipeline 50 additional time shifts of the data using 5 s steps. One time-shifted event survives, giving an expected background of 0.02 events per S3 livetime. No events pass all the analysis cuts in the unshifted data (figure 3).

6. Simulations

The efficiency of the analysis pipeline is defined as the fraction of events that would be successfully detected by the pipeline, as a function of waveform and characteristic amplitude. Preliminary detection efficiency studies were completed over a randomly selected 10% subset of the S3 data. Our simulations include 58 waveforms of various morphologies: short and long duration sine-Gaussians, Gaussians, cosmic string cusps [9], Gaussian windowed band-passed white noise, rising whistles, black-hole merger simulations [10] and supernova core collapse simulations [11–13]. In total, ∼100 000 events were injected over the S3 livetime with durations between 0.1 and 100 ms and time–frequency area $\Delta t\,\Delta f$ between 1 and 100, where unity time–frequency area corresponds to a minimal-uncertainty waveform.

Here we report detection efficiencies of the search pipeline for Gaussian injections of the form $h(t+t_0) = h_0 \exp(-t^2/\tau^2)$, with τ equal to 0.1 ms, and sine-Gaussian injections of the form $h(t+t_0) = h_0 \sin(2\pi f_0 t)\exp(-t^2/\tau^2)$, where τ is chosen according to $\tau = Q/(\sqrt{2}\pi f_0)$ with $Q = 8.9$ and f_0 assumes values of 235, 554 and 849 Hz. These simulated events are generated according to a random, isotropic sky distribution and have waveforms of purely linear polarization with random polarization angle. The strengths of the injected events are quantified by their *root-sum-square* (rss) amplitudes *at the Earth* (without folding in the antenna pattern of a detector) defined by

$$h_{\mathrm{rss}} \equiv \sqrt{\int (|h_+(t)|^2 + |h_\times(t)|^2)\,\mathrm{d}t}. \tag{5}$$

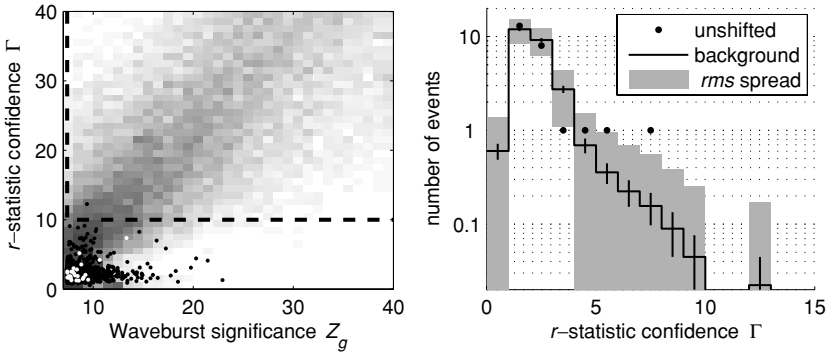

Figure 3. Left plot: measured Waveburst Z_g and r-statistic Γ values for each time-shifted event (black dots) and unshifted event (white dots). The time-shifted events used to estimate the background of our search are generated over 50 time shifts of the entire S3 data set using 5.0 s steps. Dotted lines represent the thresholds on Z_g and Γ chosen in advance to maintain a low background event rate while preserving detection efficiency for simulated events, whose density is represented by the logarithmically weighted 2D histogram. In the past, the Waveburst significance has been occasionally shown in its $\log_{10}$ representation: $Z_g/\ln(10)$. Here we follow the convention used in the S2 paper [4]. Right plot: histogram (circles) of Γ values for unshifted events with $Z_g > 7.39$. The most significant event has $\Gamma = 7.34$, below our threshold of 10; thus, no events from the analysis at zero time shift remain after all analysis cuts. Stair-step curve: estimated mean background per bin normalized to an observation time equal to that of the unshifted analysis. The black error bars indicate the statistical uncertainty on the mean background. The shaded bars represent the expected root-mean-square statistical fluctuations on the number of unshifted background events in each bin.

Table 1. Summary of the S3 pipeline sensitivity to ad hoc waveforms. Shown are the 50% detection efficiencies in terms of $h_{\rm rss}$ (strain/$\sqrt{\rm Hz}$) and in terms of the dimensionless *signal-to-noise ratio* (SNR) in the least sensitive detector. These values are averages over random sky position and polarization angle. The equivalent $h_{\rm rss}$ values for 50% detection efficiency at a comparable expected background event rate for the same waveforms in the S2 search were 1.5, 2.3, 3.9 and 4.3×10^{-20} strain/$\sqrt{\rm Hz}$ [4].

	At 50% detection efficiency	
Waveform	$h_{\rm rss}$	Minimum SNR
sine-Gaussian $f_0 = 235$ Hz, $Q = 8.9$	0.9×10^{-20}	6.0
sine-Gaussian $f_0 = 554$ Hz, $Q = 8.9$	1.3×10^{-20}	5.8
sine-Gaussian $f_0 = 849$ Hz, $Q = 8.9$	2.3×10^{-20}	7.5
Gaussian $\tau = 0.1$ ms	1.8×10^{-20}	8.4

For linearly polarized signals ($h_\times(t) = 0$), this is simply the root-sum-square amplitude of the measured strain for an optimally oriented detector. For a non-optimal orientation, the measured signal energy is diminished by an antenna factor.

The simulated events are created at constant $h_{\rm rss}$ and converted into detector-specific ADC counts using the known calibration response function and antenna pattern for each interferometer. Efficiencies at different $h_{\rm rss}$ values are evaluated by multiplying the ADC(t) time series by the appropriate factor, adding it to the raw detector data and running the combined time series through the search pipeline. Table 1 shows $h_{\rm rss}$ corresponding to 50% detection efficiency for the four reported waveforms. We find a factor of $\sim$2 improvement in overall sensitivity compared to the S2 search.

Alternatively, the efficiency can be evaluated as a function of the signal energy *received* by a given detector, taking the antenna factor into account. This can be expressed in terms of the *signal-to-noise ratio* (SNR) that would be measured by an optimal filter,

$$\mathrm{SNR}^2 = 4\int_0^\infty \mathrm{d}f \frac{|F^+\tilde{h}_+(f) + F^\times\tilde{h}_\times(f)|^2}{S(f)}, \tag{6}$$

where $\tilde{h}_+(f)$ and $\tilde{h}_\times(f)$ are the *two*-sided Fourier transforms of the two polarization components of the signal, F^+ and $F^\times$ represent the antenna factors and $S(f)$ is the *one*-sided power spectral density of the noise. Table 1 shows the SNR in the *least* sensitive detector (calculated event by event using the best noise power spectrum for each detector during the run) which yields 50% detection efficiency. The majority of the other simulated waveforms maintain 50% detection efficiency at 5–9 SNR, giving us confidence in the generality of our search pipeline with respect to match-filtering for known waveforms.

The systematic uncertainty that results from measuring the efficiency over a randomly selected 10% instead of the full data set is not expected to be large. Furthermore, a higher overlap window (finer increments in time for j and k) for the r-statistic waveform consistency test was adopted in the analysis of the full data and not implemented in the efficiency studies, implying that the efficiencies reported may be underestimated.

7. Conclusions

No gravitational-wave burst event was observed during the eight days of LIGO's S3 data that we analyse. Several improvements in the search methodology are introduced in this analysis. The waveform amplitude consistency test and the tighter r-statistic requirements for H1 and H2 both make use of the co-location and common orientation of the two Hanford detectors; information not exploited in the S2 search [4]. Additionally, the new ability of Waveburst to search at multiple time–frequency resolutions allows us to maintain sensitivity to a much larger signal space than before. These improvements are expected to be part of our future burst searches. The sensitivity of the S3 search in terms of the *root-sum-square* (rss) strain amplitude is $h_{\mathrm{rss}} \sim 10^{-20}\,\mathrm{Hz}^{-1/2}$ and reflects the most sensitive broadband search for untriggered and unmodelled gravitational-wave bursts to date.

A first interpretation of our burst upper limits within an astrophysical source context was performed in the analysis of the S2 data [4]. That analysis set the order-of-magnitude distance reach to plausible systems emitting astrophysical burst waveforms during the S2 run. Although we did not repeat this interpretation in the S3 analysis reported here, we plan to invoke astrophysical burst source population and waveform models in future searches.

Acknowledgments

The authors gratefully acknowledge the support of the United States National Science Foundation for the construction and operation of the LIGO Laboratory, and the Particle Physics and Astronomy Research Council of the United Kingdom, the Max-Planck-Society and the State of Niedersachsen/Germany for support of the construction and operation of the GEO600 detector. The authors also gratefully acknowledge the support of the research by these agencies and by the Australian Research Council, the Natural Sciences and Engineering Research Council of Canada, the Council of Scientific and Industrial Research of India, the Department of Science and Technology of India, the Spanish Ministerio de Educacion y Ciencia, the John Simon Guggenheim Foundation, the Leverhulme Trust, the David and

Lucile Packard Foundation, the Research Corporation and the Alfred P Sloan Foundation. This paper has been assigned LIGO Laboratory document number P050043-A-R.

References

[1] Abbott B *et al* (LSC) 2004 *Nucl. Instrum. Methods* A **517** 154
[2] Abbott B *et al* (LSC) 2004 *Phys. Rev.* D **69** 102001
[3] Abbott B *et al* (LSC) 2005 *Phys. Rev.* D **72** 042002
[4] Abbott B *et al* (LSC) 2005 *Phys. Rev.* D **72** 062001
[5] Klimenko S and Mitselmakher G 2004 *Class. Quantum Grav.* **21** S1819
[6] Cadonati L 2004 *Class. Quantum Grav.* **21** S1695
[7] Di Credico A (LSC) 2005 *Class. Quantum Grav.* **22** S1051
[8] Klimenko S, Yakushin I, Rakhmanov M and Mitselmakher G 2004 *Class. Quantum Grav.* **21** S1685
[9] Damour T and Vilenkin A 2005 *Phys. Rev.* D **71** 063510
[10] Baker J, Campanelli M, Lousto C O and Takahashi R 2004 *Phys. Rev.* D **69** 027505
[11] Zwerger T and Müller E 1997 *Astron. Astrophys.* **320** 209
[12] Dimmelmeier H, Font J A and Müller E 2001 *Astrophys. J. Lett.* **560** L163
[13] Ott C D, Burrows A, Livne E and Walder R 2004 *Astrophys. J.* **600** 834